Pediatr Cardiol 23:292–306, 2002
DOI: 10.1007/s00246-001-0195-8

Pediatric Cardiology

New Ultrasound Methods to Quantify Regional Myocardial Function in Children with Heart Disease

F. Weidemann, B. Eyskens, G.R. Sutherland

Departments of Cardiology and Pediatric Cardiology, University Hospital Gasthuisberg, Herestraat 49, B-3000 Leuven, Belgium

Abstract. From a temporally resolved radio-frequency data set, a series of new developing indices of regional myocardial deformation can be measured. These may be important new data sets to quantify regional radial and long axis function of the left or right ventricle in children with acquired or congenital heart disease. Using color Doppler methodology unidimensional regional myocardial strain rates (SR) and natural strain (ε) can now be calculated from local myocardial velocity data sets. Normal regional velocity, SR, and ε values have already been determined in older children and should form the database for studies into acquired or congenital heart disease in this age group. Neonatal and infant values have yet to be determined. This article will present preliminary data on the potential clinical value of ultrasonic regional SR and ε imaging in children and will discuss the close interrelation of these new regional function parameters with an alternative approach to quantification: the measurement of local cyclical changes in integrated backscatter levels.

Key words: Ultrasound, new methods

Echocardiography is a well-established clinical tool for the noninvasive assessment of regional and global left ventricular (LV) function in children [9]. It may be based on a qualitative or quantitative approach. The qualitative approach is based on the visual interpretation of local radial endocardial excursion combined with the assessment of local wall thickening/thinning characteristics. However, the visual interpretation of either endocardial excursion or myocardial thickening is nonquantitative and is both subjective and experience-dependent [22]. The current standard approach to quantifying regional function is based either on the measurement of regional radial thickening/thinning by parasternal M-mode echocardiography or the new anatomical M-mode technique, which during postprocessing of the digital ultrasound data implants a user defined M-mode into a real time two-dimensional data set. Measurement of regional radial function by the conventional M-mode technique is only applicable to the relatively few LV segments that can be insonated at 90 degrees from the parasternal approach. This limitation has been somewhat improved by the introduction of the anatomic M-mode technique, which allows an M-mode to be implanted into data sets obtained from an apical transducer position. However, this latter approach has not proved to be an optimal solution.

For long axis function assessment, the only ultrasound technique currently applicable is M-mode measurement of atrioventricular plane displacement. However conventional M-mode measurement of long axis ring excursion only quantifies the overall shortening or lengthening of the subtended myocardial wall and does not measure the local long axis deformation of each of the wall segments.

Another approach used to study radial function has been color kinesis. In this technique, radial endocardial motion is tracked. The tracking algorithm is based on border detection of the integrated backscatter signal from the blood/pool endocardial interface [10]. However, radial motion does not measure local deformation and may be influenced by overall heart motion.

In theory, to characterize regional myocardial function accurately, it is necessary to measure local deformation in three direction, i.e, radial, long axis, and circumferential. Currently, such local three-dimensional strain rate (SR) and strain (ε) data can only be measured in children using magnetic resonance tagging. This is both cumbersome and labor-intensive. An alternative bedside approach based on ultrasound might be more clinically effective. Current

Correspondence to: G.R. Sutherland; *email:* george.sutherland@uz.kuleuven.ac.be

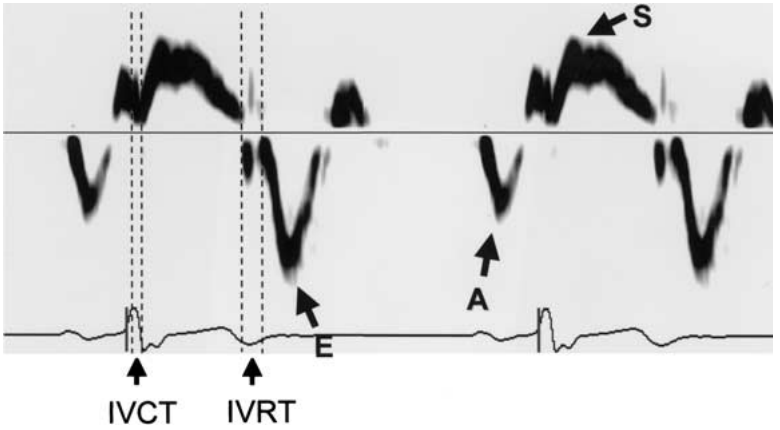

Fig. 1. An example of a normal myocardial spectral pulsed Doppler velocity profile obtained from a basal myocardial segment from a normal child. This was recorded from an apical transducer position and therefore examines long axis function. In systole the myocardium is moving toward the transducer (*above the baseline*). In early and late diastole the myocardium is moving away from the transducer. *A*, late diastole; *E*, early diastole; *IVCT*, Isovolumetric contraction period; *IVRT*, Isovolumetric relaxation period; *S*, systole

ultrasound transducers acquire only unidimensional data sets. However, a unidimensional approach will allow the acquisition of both radial and long axis ultrasound data from many ventricular segments by insonating individual segments from two differing transducer positions—a parasternal position for radial data and an apical position for long axis data. The ultrasound data thus obtained may be processed to derive regional velocity profiles using the new methodology of Doppler myocardial imaging (DMI). From two local velocity data sets it is now possible to calculate the unidimensional regional deformation indices SR and ε. It remains to be seen whether such unidimensional data sets (as opposed to the three-dimensional data sets acquired by magnetic resonance imaging) will be sufficiently robust and reproducible to characterize regional deformation in both health and disease to allow improved clinical decisions on management to be made. Yet one thing is clear: better methods are required to quantify both systolic and diastolic regional function in pediatric patients with acquired or congenital heart disease. This is especially true for right ventricle (RV) function.

Technical Aspects of DMI

DMI is a relatively new ultrasound technique that can quantify intramural myocardial velocities by the detection of consecutive phase shifts of the ultrasound signal reflected from contracting myocardium [8, 26]. It is based on the same principles as conventional Doppler blood flow imaging and makes use of the two main differences between the signal derived from blood and tissue. First, blood velocities in the ventricular cavities and great vessels are relatively high and normally reach 100–150 cm/s. Myocardium moves at much lower velocities than blood flow, typically 5–15 cm/s. Second, the amplitude of the Doppler signal obtained from the myocardium is significantly higher than the blood velocity signal. Thus to implement DMI signal processing, signals with lower velocities and higher amplitudes are selected, whereas those with higher velocities and lower amplitudes arising from the blood pool are filtered out by thresholding algorithms. Myocardial velocities may be recorded using either spectral pulsed or color Doppler signal processing. In spectral pulsed-wave myocardial Doppler imaging (Fig. 1), a sample volume of some 6–8 mm is placed in the center of the region of myocardium to be examined. This method allows the resolution of peak velocities within the relatively large regions of interest that move through the sample volume during the cardiac cycle. The method has a very high temporal (>250 samples/s) but poor spatial resolution. For the color Doppler method, mean Doppler shift, and hence velocity is calculated by autocorrelation signal processing and can be displayed either as a color-coded M-mode or two-dimensional data set. This technique measures mean velocities (not peak) with both high temporal (150 frames/s) and high spatial resolution in the axial direction. The color Doppler myocardial signal is usually displayed superimposed on the underlying M-mode or two-dimensional grayscale image (Fig. 2) and displayed in real time.

According to the blood pool Doppler convention of displaying directional information, tissue velocities directed toward the transducer are similarly coded red to yellow, and motion away from the transducer is coded blue to green. As the DMI technique is based on resolving the phase shift of the returning signal from the interrogated tissue, the ultrasonic image is relatively independent of the amplitude of the returning signal and is thus little affected by the attenuating effect of the chest wall. Thus it is possible to obtain diagnostic-quality DMI images from patients who would be considered poorly echogenic as a result of chest wall attenuation effects on standard grayscale imaging.

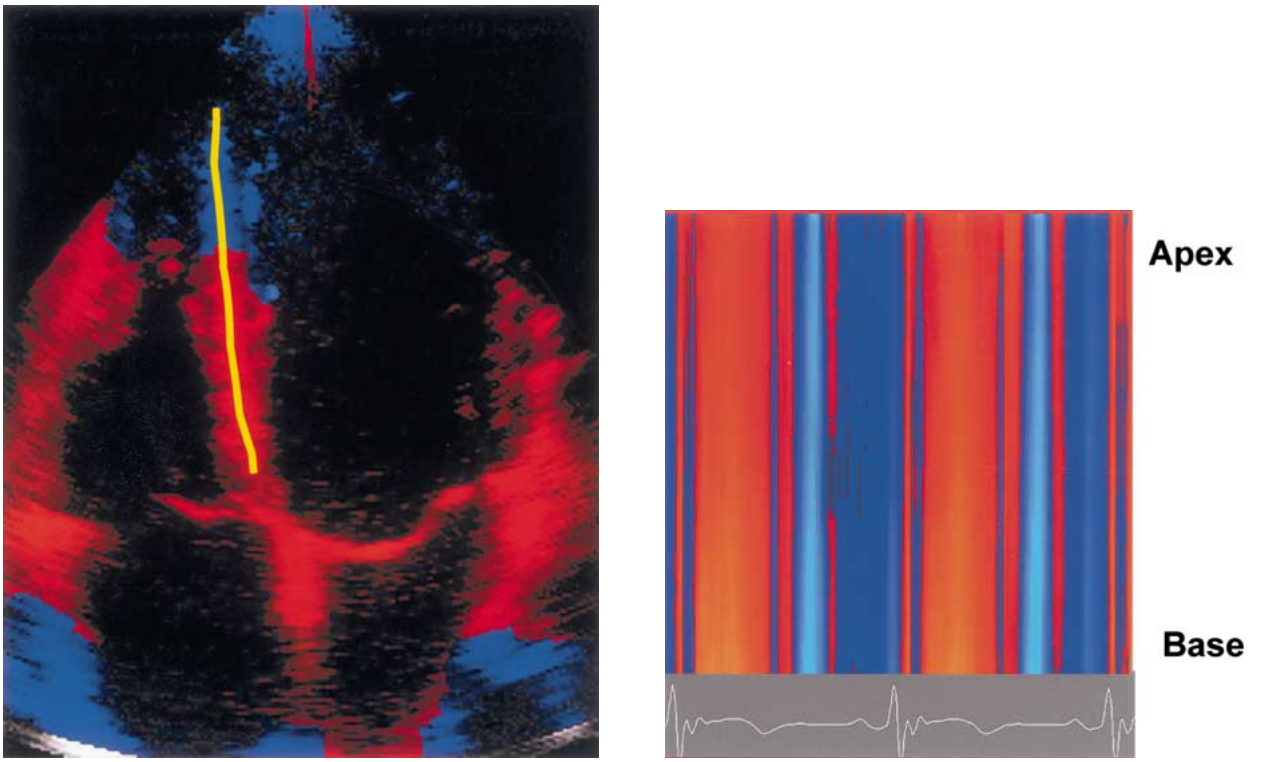

Fig. 2. An example of a normal two-dimensional and septal M-mode color Doppler velocity display from a child. **Left:** In this apical four-chamber image the color Doppler velocity signals are superimposed on the standard two-dimensional grayscale image. **Right:** The color Doppler velocity signals are superimposed on a curved M-mode drawn through the long axis of the interventricular septum (yellow line). To derive velocities only from the myocardium, the region of interest is continuously positioned within the segments being interrogated using a semi-automatic tracking algorithm. For the *SR* estimation, the color-curved M-mode septal data is displayed with the apex superiorly and the base inferiorly. Note that there is a marked base-apex gradient for all systolic and diastolic velocities with the highest velocities at the cardiac base (bright red in systole; bright blue in diastole) and lowest velocities at the apex. This is a constant finding in all LV and RV walls in normal individuals as the apex is relatively fixed and the base is moving toward the apex during systole.

Potential Clinical Applications of DMI in Pediatric Cardiology

Regional Myocardial Velocities: Normal and Abnormal Findings

In 1996 Rychik et al. [25] published the first article on the application of DMI in children. They described normal pulsed-wave Doppler velocity measurements of LV wall motion in healthy children and reported normal systolic and diastolic peak velocities derived from the mitral annulus and posterior wall. However, their study was based on only a small number of patients. A more extensive study to define normal values, which included 165 healthy children (age range 4–18 years), has subsequently been published by Kapusta et al. [16]. This study used color-coded DMI to record normal peak systolic and early and late diastolic velocities in all LV and RV segments. The authors also described the differences in trans-myocardial velocity between the left and right side of the interventricular septum, as well as between the endocardium and epicardium of the LV posterior wall (the local transmural velocity gradient [7]. These normal velocity values (Table 1) were established to serve as a reference for subsequent clinical studies on impaired myocardial function in children [16]. A further study, reporting normal pulsed Doppler values has been published by Mori et al., who determined the myocardial velocities in 131 healthy children over a wide age range (two months to 19 years). In contrast to Kapusta et al., the authors showed that normal myocardial velocity values change with age and are influenced by heart rate [20]. However, further studies are still needed to describe the complete range of normal values in neonates and infants. Indeed, the issue of heart rate versus age-dependency in the pediatric age range remains to be clarified.

A number of other clinical studies have examined the potential use of pulsed Doppler myocardial velocities in assessing children with heart disease. These have been based on determining regional myocardial function from local velocity

Table 1. Median (and their 5th–95th percentile) of peak myocardial velocities (cm/s) obtained from long axis view (n = 160)

	Peak systolic velocity (S)	Peak early diastolic velocity (De)	Peak late diastolic velocity (Da)	De/Da ratio	De/S ratio
RVAW	−2.3 (−0.7 – −4.2)	3.2 (1.2–6.0)	1.0 (0.2–2.4)	3.0 (1.1–10.8)	−1.4 (−0.6 – −3.0)
IVSR	−2.1 (−0.9 – −3.5)	3.6 (1.5–6.4)	1.5 (0.6–2.9)	2.5 (0.7–7.9)	−1.6 (−0.8 – −5.9)
IVSL	−3.2 (−2.1 – −4.5)	4.9 (3.0–8.4)	1.9 (0.8–3.5)	2.6 (1.1–7.4)	−1.5 (−0.8 – −3.2)
LVPWen	3.9 (2.4–5.8)	−9.8 (−5.3 – −15.0)	−1.2 (−0.4 – −3.2)	8.3 (2.3–27.0)	−2.4 (−1.6 – −3.7)
LVPWepi	2.2 (1.1–3.5)	−3.7 (−1.8 – −6.7)	−0.7 (−0.2 – −2.4)	5.6 (1.0–19.0)	−1.8 (−0.8 – −3.6)

De/Da and De/S ratios were calculated.

Median (and their 5th–95th percentile) of peak myocardial velocities (cm/s) obtained from apical four-chamber view (n = 160)

	S	De	Da	De/Da ratio	De/S ratio
RVW basal	12.8 (10.7–16.5)	−16.2 (−12.6 – −21.1)	−8.6 (−5.5 – −12.1)	1.8[a] (1.3–3.0)	−1.3[a] (−1.0 – −1.6)
mid	10.9 (8.6–13.7)	−13.9 (−9.4 – −17.7)	−7.1 (−4.7 – −10.0)	1.9[a,b] (1.3–3.0)	−1.2[a] (−0.9 – −1.6)
apical	8.0 (5.7–10.8)	−10.8 (−7.0 – −14.3)	−5.3 (−3.6 – −7.8)	2.0[b] (1.2–3.2)	−1.4[b] (−0.9 – −1.9)
IVS basal	8.1 (6.5–9.8)	−14.3 (−11.2 – −18.5)	−5.8 (−4.4 – −7.9)	2.5[a] (1.7–3.6)	−1.8[a] (−1.5 – −2.2)
mid	6.1 (4.7–7.5)	−13.0 (−9.2 – −16.2)	−4.9 (−3.5 – −6.5)	2.7[b] (1.8–3.8)	−2.1[b] (−1.4 – −2.8)
apical	4.6 (3.1–6.4)	−9.0 (−5.9 – −12.7)	−3.7 (−2.4 – −5.0)	2.5[a] (1.6–3.8)	−2.0[b] (−1.3 – −3.0)
LVW basal	9.7 (6.3–13.5)	−17.6 (−13.0 – −23.0)	−5.5 (−3.8 – −8.0)	3.3[a] (2.1–4.7)	−1.8[a] (−1.3 – −2.6)
mid	9.5 (6.2–13.3)	−15.9 (−10.0 – −21.0)	−4.6 (−3.2 – −7.1)	3.3[a] (2.1–5.0)	−1.6[b] (−1.1 – −2.3)
apical	8.7 (5.0–12.4)	−10.7 (−6.5 – −15.3)	−3.9[†] (−1.9 – −5.8)	2.8[†b] (1.7–4.5)	−1.2[c] (−0.8 – −1.8)

De/Da and De/S ratios were calculated.
[†]Number of subjects = 140.
Different letters indicate significant differences between positions.
For each wall and each ratio, the overall significance level is 5%.
Source: Reprinted by permission of Elsevier Science from Kapusta et al. (2000) "Assessment of myocardial velocities in healthy children using tissue Doppler imaging," *Ultrasound Med Biol 26*:229–237 by World Federation of Ultrasound in Medicine and Biology.

profiles. Different clinical problems have been explored. Pacileo et al. [21] investigated regional diastolic function in children with hypertrophic cardiomyopathy and studied the effect of verapamil treatment. They concluded that the beneficial effects of verapamil are more related to reduction in diastolic asynchrony than to significant changes in diastolic velocities of the myocardial fibres. Kapusta et al. [17] studied myocardial dysfunction after anthracyclin treatment in children following cancer treatment. They reported lower late diastolic myocardial velocities and lower transmyocardial systolic and diastolic velocity differences in late survivors of childhood cancer compared to a normal population. Vogel et al. investigated inhomogeneous contraction patterns both in patients after a Fontan procedure [28] and after tetralogy of Fallot correction [29]. In patients with tetralogy of Fallot they found right ventricular wall motion abnormalities to be associated with repolarization-depolarization abnormalities. Iwasaki et al. [13] used the technique to assess paradoxical motion of the ventricular septum in children with an atrial septal defect. Their study showed that the degree of this displacement correlated with that of volume overload of the RV. Most of these reports contained promising preliminary data, which suggested that this new quantitative approach could be of added value to current methods of assessing regional function in children with heart disease.

The Rationale for Development of Ultrasonic Strain Rate/Strain Imaging

One of the major disadvantages of regional function quantification by detecting the velocity of myocardial motion is that velocity profiles are detected with respect to transducer position and may be influenced by overall heart motion, cardiac rotation, and motion induced by tethering to adjacent myocardial segments [19]. This means that a regional velocity profile may reflect not only motion induced by local myocardial contraction and relaxation but also passive translation and rotation of the segment interrogated. To overcome this problem, the technique of ultrasonic *SR*-imaging or so called rate of deformation imaging, has been developed to measure the "true" local rate of myocardial deformation [11].

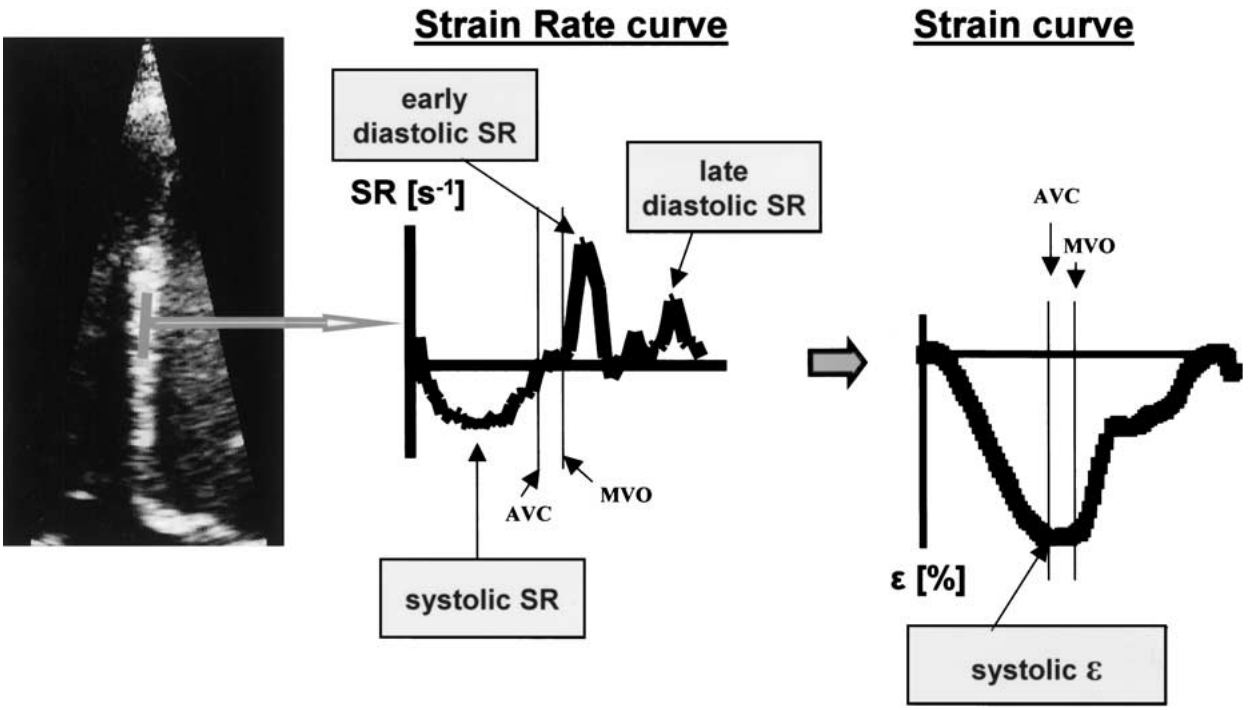

Fig. 3. An example of a long axis *SR* and ε profile extracted from the mid-septal segment of a normal child. **Left:** An apical four-chamber image with the area of computation set in the mid-septal segment. **Middle:** The SR profile derived from the two-dimensional image with myocardial shortening occurs in systole (negative peak) and lengthening in early and late diastole (positive peaks). **Right:** The ε profile derived by integration of the SR curve with shortening in systole and lengthening in diastole. As the time reference for this deformation profile over one heart cycle is end-diastole, the ε curve is negative in systole (myocardial shortening) and in diastole (myocardial lengthening) the curve is returning to the baseline point, *AVC*, aortic valve closure; *SR*, strain rate; *MVO*, mitral valve opening; ε, strain.

Technical Aspects of Strain Rate/Strain Imaging

From a standard color DMI velocity data set, two deformation parameters can be calculated: local unidimensional SR and its integral, local ε.

Regional Strain Rate: This corresponds to the rate of the deformation of an object. Local myocardial *SR* (expressed in s^{-1}) can be calculated from the spatial gradient in velocities recorded between two neighboring points in the tissue (point *A* and *B* with velocities v_A and v_B):

$$SR = \frac{v_B - v_A}{L}$$

with *L* reflecting the distance between the point *A* and *B* [4].

The distance between the two points (area of computation) is normally 4–5 mm for the radial direction and 8–9 mm for the longitudinal direction. When a segment thickens in the radial direction, *SR* is defined to have a positive value. When a segment thins in the radial direction, it is characterized by a negative value. Thickening/thinning parameters derived by *SR* imaging describe only radial deformation and are equivalent to those derived by measurement of the local radial myocardial velocity gradient [7]. Long axis changes in regional deformation (measured from an apical transducer position), are better described by the terms "shortening" in systole (negative *SR* value) and "lengthening" in diastole (positive *SR* value) (Fig. 3). A color display using a transition from yellow to red for increasingly more negative *SR* (i.e. thinning/shortening) and a transition from cyan to blue for an increasingly more positive *SR* (i.e., thickening/lengthening) has been chosen to detect *SR* changes in standard two-dimensional and M-mode (Fig. 4) displays. In addition, *SR*s that approach zero are colored green. This facilitates the visual appreciation of myocardial regions or time periods with normal deformation (red/blue), reduced deformation (yellow/cyan), or no deformation (green).

Regional Strain: Regional ε values can be obtained by integrating the regional *SR* curve over time, ε defines the amount of local deformation caused by an applied force [4]. Myocardial radial ε describes local

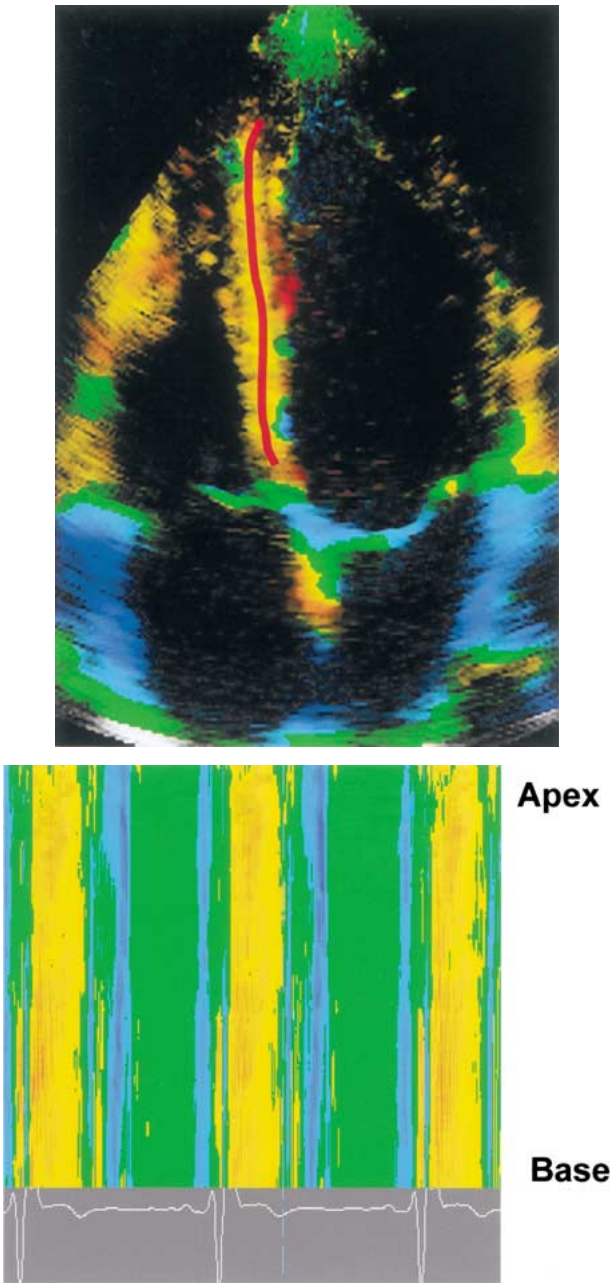

Fig. 4. An example of a two-dimensional and curved M-mode color Doppler long axis SR image from a normal child. **Top:** The color Doppler SR signals are superimposed on two-dimensional apical four-chamber view. **Bottom:** The color Doppler SR signals are superimposed on a long axis curved M-mode of the septum (red line). To derive SRs only from the myocardium, the region of interest is continuously positioned within the segments being interrogated using a semi-automatic tracking algorithm. The color-curved M mode is displayed from the apex (superiorly) to the base (inferiorly) of the septum. Note the homogenous distribution of SRs throughout the septum compared to the corresponding base-apex gradient displayed in Fig. 2.

thickening in systole (positive ε value) and thinning in diastole (negative ε value). Long axis ε is described by the terms "shortening" in systole (negative ε value) and "lengthening" in diastole (positive ε value).

Both regional thickening/shortening and thinning/lengthening can be measured during the cardiac cycle. The ultrasound technique as currently formatted measures the instantaneous change in segment length. This is the natural ε value [4], which is expressed as a Percentage and is described by the equation

$$\epsilon_N = \int_{t_o}^{t} SRdt$$

where t_0 is a reference time point, t is the instant time point, and dt is an infinitesimally small time interval.

An alternative approach to measuring regional deformation is to use magnetic resonance imaging (MRI) tagging techniques. These have both advantages and disadvantages compared to the ultrasound method described herein. MRI tagging techniques can resolve three-dimensional regional ε, as ε can be resolved at sampling rates of 15–20/s. However, the calculation of regional *SR* requires sampling rates of greater than 100/s. Thus resolved *SR* curves cannot be obtained with the current MRI low real-time sampling rates. With ultrasound, real-time sampling rates of >350/s are now available and thus one-dimensional *SR* can be resolved. However, the measurement of *SR* by ultrasound is angle-dependent. Both MRI and ultrasound deformation data sets have the same axial spatial resolution, but ultrasound has a much inferior lateral spatial resolution. Presently it is not clear whether it is better to resolve both ε and *SR* in one dimension or to fully resolve an ε data set in three dimensions. Future correlative studies will determine this. However, to date MRI tagging has been applied in only a limited number of studies in patients with congenital heart disease.

Timing of Global Heart Events

When analyzing regional function it is always necessary to compare the local measurements to global timing events, because in bundle branch block, ischemia, and cardiomyopathies a significant amount of thickening can occur after aortic valve closure. This is wasted myocardial work. Thus for each segment both systolic ε and postsystolic ε should be measured. The basal septal color DMI velocity curves can be used to time end-diastole (onset of isovolumic contraction) and end-systole (aortic valve closure) for each cardiac cycle. Both mechanical events induce a clearly identifiable rapid directional change in the basal septal

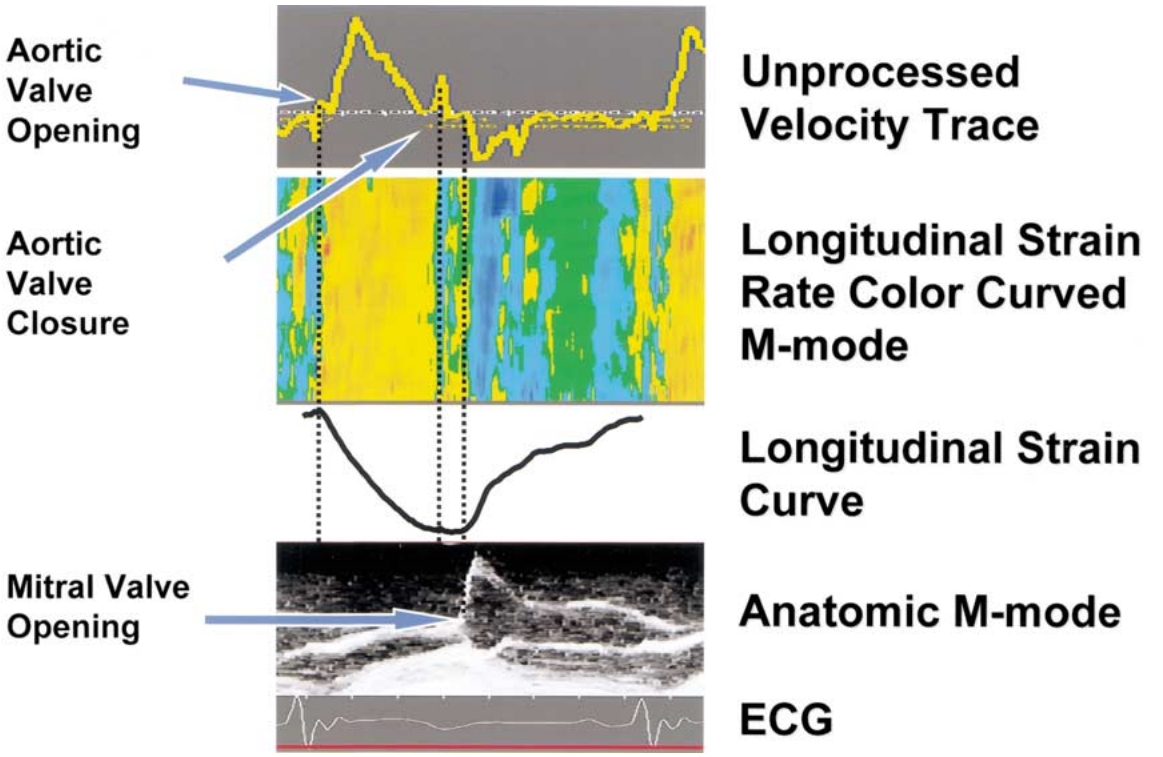

Fig. 5. An example of how to time global cardiac mechanical events. An unprocessed velocity trace from the basal septum is used for the timing of aortic valve opening and closure. Both mechanical events induce a clearly identifiable rapid directional change in the basal septal velocity curve. An anatomic M-mode over the tips of the mitral valve leaflets is used for the timing of mitral valve opening. Postprocessing software will allow these global event markers to be imported into the local *SR* and ε curves. Note the myocardial shortening in systole *(orange band)* and myocardial lengthening in early and late diastole *(blue bands)*.

velocity curve, which correlates with the timing of the rapid upstroke and peak negative left ventricular dP/dt data, respectively [15]. To define the onset of filling (onset of diastole) the timing of mitral valve opening can be obtained using an anatomic grayscale M-mode cursor positioned visually in the underlying grayscale data set at the level of mitral valve leaflets (Fig. 5).

Current Applications of Strain Rate/Strain Imaging

In vitro phantom studies had shown an excellent correlation between calculated *SR*s and measured material deformation properties [12]. In experimental work Urheim et al. [27] recently validated ultrasound ε measurements by comparison with microcrystal ε measurements and confirmed that the ultrasound deformation parameter is less influenced by tethering effects than regional velocity estimation. Thus ε appears to represent true local deformation changes.

In adult patients, regional *SR* and ε calculation have already been shown to quantify regional myocardial deformation both in acutely ischemic myocardium [6, 14] and in chronic infarcted myocardium [11, 30].

Edvardson et al. [6] demonstrated that in patients undergoing coronary angioplasty, *SR* imaging is more accurate than peak velocity measurement in detecting systolic regional myocardial dysfunction induced by the transient coronary artery occlusion.

In pediatric cardiology these new ultrasound indices could be an important new noninvasive bedside approach to the quantification of local myocardial deformation in both acquired or congenital abnormalities. Current post processing algorithms now allow data to be postprocessed in a matter of minutes after real-time data acquisition. Normal systolic and diastolic *SR* and ε values from all LV segments in healthy children have already been defined (Tables 2 and 3) [32].

Clinical Examples of the Potential Value of Strain Rate/Strain Imaging in Pediatric Patients

Regional LV Function:

- LV Ischemia: In an infant with abnormal left coronary artery arising from the pulmonary artery *SR*

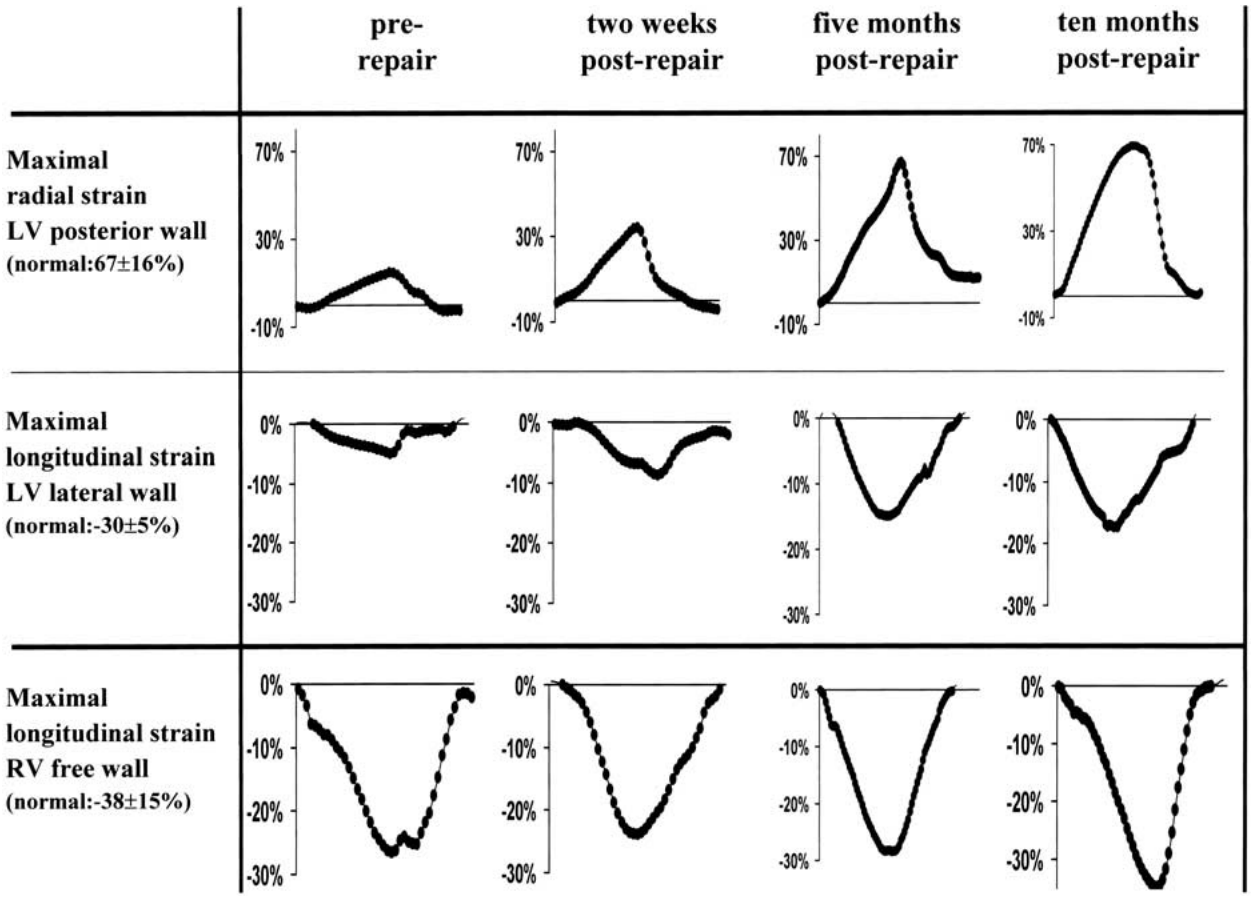

Fig. 6. Maximal systolic strain as a parameter for the regional myocardial systolic function in an infant with abnormal left coronary artery arising from the pulmonary artery pre- and postrepair. The maximal radial systolic strain of the left ventricular posterior wall is markedly reduced prerepair, improves immediately postrepair, and is normal after 5 months. The maximal long axis systolic strain in the left ventricular mid segment of the lateral wall is reduced pre- and improves postrepair but is still not normal after 10 months. The maximal long axis systolic strain of the mid segment of the right ventricular free wall is normal prerepair, slightly reduced 2 weeks postrepair, and recovered to normal in the 10 months follow-up. *LV*, left ventricle; *RV*, right ventricle. (From Mertens et al. (2001) *Cardial Young* 2001; used by permission.)

and ε measurements were used to assess and monitor LV and RV function pre- and after coronary reimplantation [18]. In this study both regional radial and long axis myocardial function of the LV was homogeneously reduced prerepair, and postrepair the time course of their recovery differed with regional radial function recovery occurring earlier and more completely in contrast to long axis function (Fig. 6).

- Hypertrophy Cardiomyopathy: The fact that *SR* ε imaging can quantify both radial and long axis LV function and the possible difference between both is illustrated by data obtained from a 6-year-old child with a non/obstructive hypertrophic cardiomyopathy (Fig. 7). This child had normal radial function of LV posterior wall with normal myocardial thickening in systole (systolic ε: 50%) and normal myocardial thinning in early diastole (peak early diastolic *SR*: $-8\ s^{-1}$). In contrast LV long axis systolic shortening and diastolic lengthening of the posterior wall were markedly reduced (systolic ε: −9%; peak early diastolic *SR*: $1\ s^{-1}$). The *SR* color-curved M-mode confirmed normal radial function and almost no long axis shortening in systole and lengthening in diastole (Fig. 7).
- Aortic Stenosis: As *SR* and ε indices quantify regional deformation they can also be used to demonstrate heterogeneity in regional function. In an infant with congenital aortic stenosis balloon valvuloplasty was performed in the first month of life. The ultrasound-based *SR* imaging at 13 years of age showed very heterogeneous long axis deformation properties in the LV. The systolic ε in the apical septal segment was normal (−21%) and in the basal septal segment slightly reduced (16%). In the posterior wall the long axis systolic ε was reduced to −6% in the basal segment and −2% in the apical segment. Surprisingly the radial systolic function of the posterior wall was normal (60%). Using the SR color-curved M-mode from the apex

Table 2. Systolic and diastolic strain rate (s^{-1}) and systolic strain (%) for regional LV longitudinal function

	Strain rate		Strain	
	Systolic	Early diastolic	Late diastolic	Systolic
Septum **(4CH):**				
Base	−1.8 ± 0.6	2.6 ± 0.9	1.4 ± 0.6	−24 ± 06
Mid	−1.9 ± 0.6	2.3 ± 0.9	1.3 ± 0.7	−24 ± 06
Apic	−1.7 ± 0.3	2.8 ± 0.9	1.8 ± 0.3	−24 ± 06
Lateral **(4CH)**				
Base	−2.2 ± 1.1	2.7 ± 1.1	1.9 ± 1.2	−26 ± 11
Mid	−2.1 ± 1.0	3.4 ± 1.5*	1.5 ± 0.8	−26 ± 08
Apic	−1.9 ± 0.7	3.3 ± 1.4	1.0 ± 0.7†	−25 ± 07
LV inferior **(2CH)**				
Base	−1.7 ± 0.5	3.0 ± 1.0	1.4 ± 0.7	−24 ± 06
Mid	−1.9 ± 0.6	2.7 ± 1.4	1.4 ± 0.7	−24 ± 09
Apic	−2.0 ± 0.5	3.5 ± 1.4	1.2 ± 0.5	−26 ± 09

Apic, apical segment; base, basal segment; LV, left ventricular; mid, mid-wall segment; 4CH, apical 4-chamber view; 2CH, apical 2-chamber view.
*$p < 0.001$ versus corresponding segment in septum.
†$p < 0.5$ versus apic versus basal segment of the same wall.

Table 3. Systolic and diastolic strain rate (s^{-1}) and strain (%) for regional LV radial function

	Strain rate		Strain	
	Systolic	Early diastolic	Late diastolic	Systolic
SA (post)	3.7 ± 1.1	−8.0 ± 2.3	−2.2 ± 1.3	58 ± 12
SA (post)	3.7 ± 0.9	−7.8 ± 2.1	−2.2 ± 1.2	56 ± 11

LA (post), posterior wall in the parasternal long axis; SA (post), posterior wall in the parasternal short axis.

to the base in the septum and the posterior wall, a very patchy *SR* pattern confirmed the heterogeneous long axis deformation properties (Fig. 8). This is an excellent example of the potential clinical value of this new quantitative approach to regional function as on both visual inspection and on measuring LV function by the standard parasternal approach would have been described as normal.

Regional RV Function:

- Subpulmonary RV: As well as using this technique to quantify LV function, regional long axis RV function can be measured by SR/ε imaging. In a child with severe pulmonary stenosis, SR/ε imaging showed homogeneous reduced systolic ε values in the basal (−14%), mid (−12%), and apical segments (−11%) of the RV free wall (normal systolic ε values: basal = 36 ± 11%, mid = 45 ±13%, apical = 34 ± 11%) (Fig 9).

In children after correction of tetralogy of Fallot, the deformation properties in the RV free wall usually remain abnormally reduced despite the volume loading due to pulmonary regurgitation. This is illustrated in a 12-year-old patient 11 years after surgical correction with moderate pulmonary regurgitation and no residual pulmonary stenosis. In this patient the systolic *SR* and ε in all the RV segments were markedly reduced (systolic ε in the RV mid segment: −20%). The *SR* color-curved M-mode of the RV free wall revealed uniform low *SR* in systole (Fig. 10; yellow band in systole) and a long diastasis period with almost no diastolic deformation (Fig. 10; green band in mid diastole). This suggests both significant systolic as well as diastolic RV dysfunction in this patient after correction.

In pulmonary stenosis we have already demonstrated that the technique can be useful in quantifying RV function. This is true not only for pressure-loaded hypertrophied RVs but also for thin-walled, volume-loaded ventricles. In a 4-year-old child with an atrial septal defect and significant left-to-right shunt, the deformation properties in the RV free wall were estimated before and 1 month after occlusion by an Amplatz septal occluder (Fig. 11). The *SR* color-curved M-mode showed homogeneously increased systolic (Fig. 10; dark orange band) and diastolic *SR*s (Fig. 11; dark blue band) in the RV free wall at baseline. In addition the systolic ε in the mid RV free wall seg-

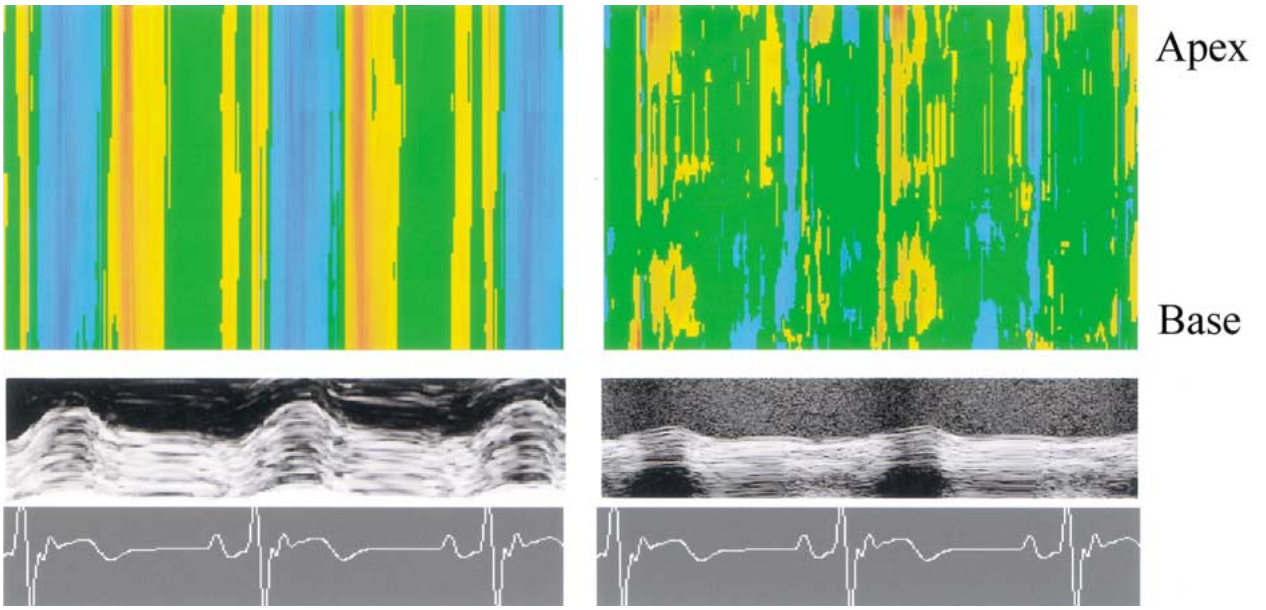

Fig. 7. An example of the difference or radial and long axis function in a 6-year-old child with a nonobstructive hypertrophic cardiomyopathy. **Left:** The color-coded radial SR M-mode of the posterior wall (above) with the corresponding grayscale M-mode *(below)*. Note the normal radial thickening in systole (blue band) and thinning in diastole *(yellow band)*, which is confirmed by the normal radial thickening of the posterior wall in the grayscale M-mode. **Right:** The color-coded long axis curved SR M-mode of the posterior wall from the apex to the base (above) with the corresponding grayscale M-mode over the posterior ring *(below)*. Note the non-homogeneous SR pattern with reduced myocardial shortening in systole *(yellow patches)* and reduced myocardial lengthening in diastole (blue patches). This is confirmed by the reduced long axis posterior wall ring motion in the grayscale M-mode. *SR*, strain rate.

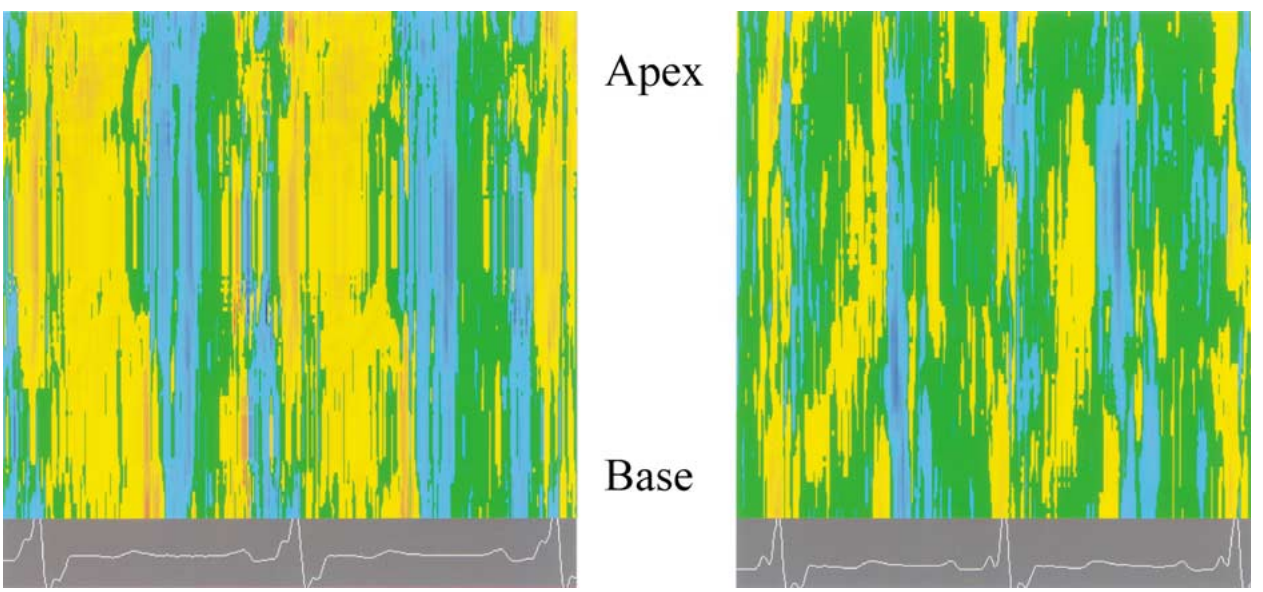

Fig. 8. An example of SR imaging in a 13-year-old child with congenital aortic stenosis who underwent balloon valvuloplasty in the first month of life. **Left:** The color-coded long axis curved SR M-mode of the septum from the apex to the base. **Right:** The color-coded long axis curved SR M-mode of the posterior wall from the apex to the base. Notice the very heterogeneous long axis deformation properties in the LV with normal systolic myocardial shortening only in the apical septal segment *(yellow band)* and almost no systolic shortening in the posterior wall. This example shows that the color-coded curved SR M-mode might be useful to get visual information about the heterogeneity in regional myocardial function. *SR*, strain rate.

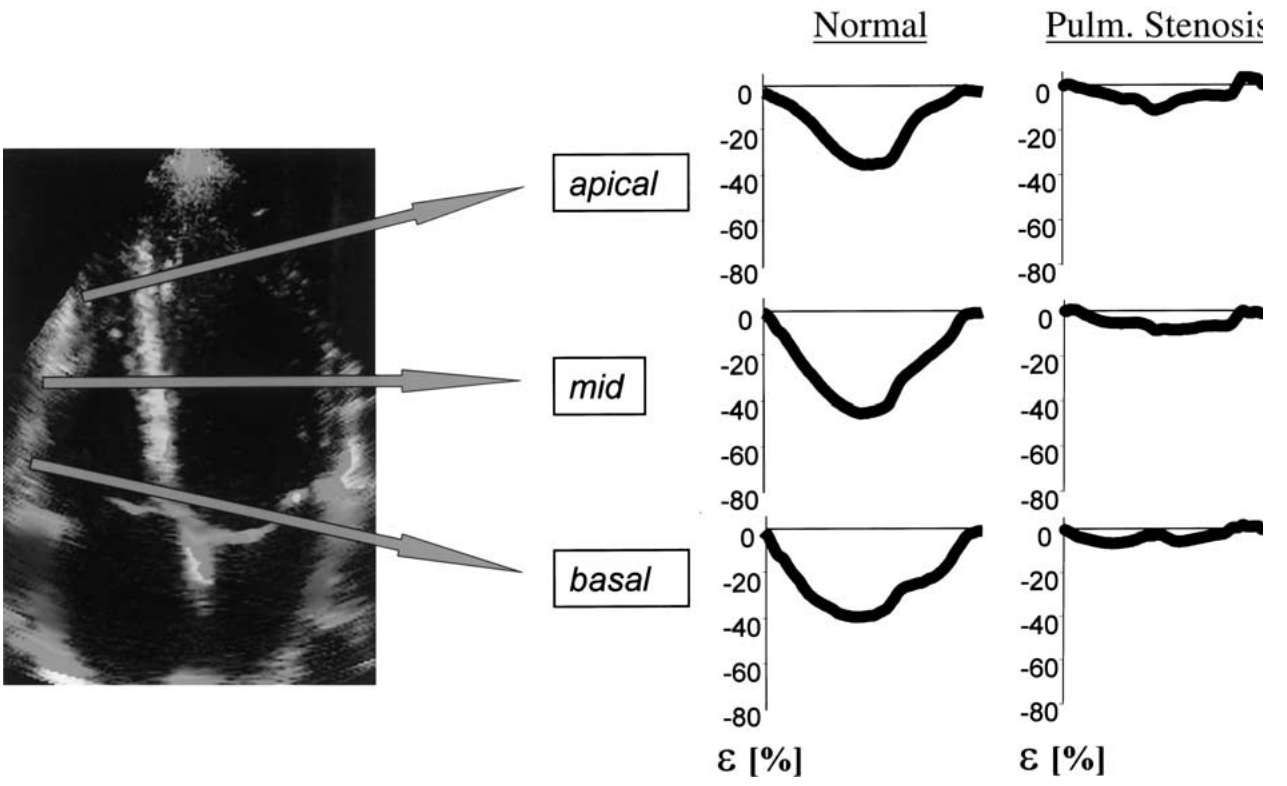

Fig. 9. An example of long axis ε abnormalities in a patient with severe pulmonary stenosis. **Left:** An apical four-chamber view showing the segments of the RV free wall from which the corresponding ε curves were extracted. **Middle:** The corresponding long axis regional ε curves from the RV basal, mid, and apical segment of a healthy child. **Right:** The long axis regional ε curves from the RV basal, mid, apical segment of the patient with severe pulmonary stenosis where the ε is homogeneous reduced. ε = strain.

ment was markedly increased to −70%. This was due to volume loading of the RV by the large left-to-right shunt. One month after defect closure by a device, *SR*/ε imaging confirmed normal *SR* and ε values in all three RV segments. This example indicates that *SR* imaging might be useful for monitoring myocardial function pre and post interventions.

- The RV as the Systemic Ventricle: In another clinical study *SR* and ε measurements have been shown to identify and quantify normal and abnormal systemic ventricle regional function in children after a Senning procedure [31]. In the post-Senning patients, RV regional systolic and diastolic long axis function indices were reduced compared to *SR*/ε values in low-pressure subpulmonary RVs. Moreover, the *SR* and ε values within the RV free wall were very homogeneous and similar to the normal systemic LV free wall. The homogeneity in ε values in these systemic RVs suggested that local deformation parameters could be used in the assessment of global function. This was studied in a group of post-Senning children by correlating the ε values of the basal segment of the systemic RV free wall with the RV ejection fraction assessed by MRI (Fig. 12). The good correlation suggested that regional *SR* and ε might be useful new parameters for the quantification of both regional and global RV function and could be used in the long-term follow-up of these patients.

Limitations of DMI and *SR*

Currently, *SR* imaging offers only a unidimensional real-time measurement of regional *SR* and ε in either the radial or long axis direction. Current developments in both hardware (two-dimensional arrays) and beam forming allied to the implementation of cross-correlation methods of deriving regional *SR* and ε from the raw radio frequency data may allow the real-time measurement of either two- or three-dimensional *SR*'s and ε's [5].

As with any Doppler-based technique, the usual limitations inherent in the angle dependency of velocity estimation apply to color Doppler–based *SR*/ε estimation. Therefore meticulous care should be taken to align the ultrasound beam as near parallel as possible (at least within 15 degrees) to the interrogated direction of myocardial motion.

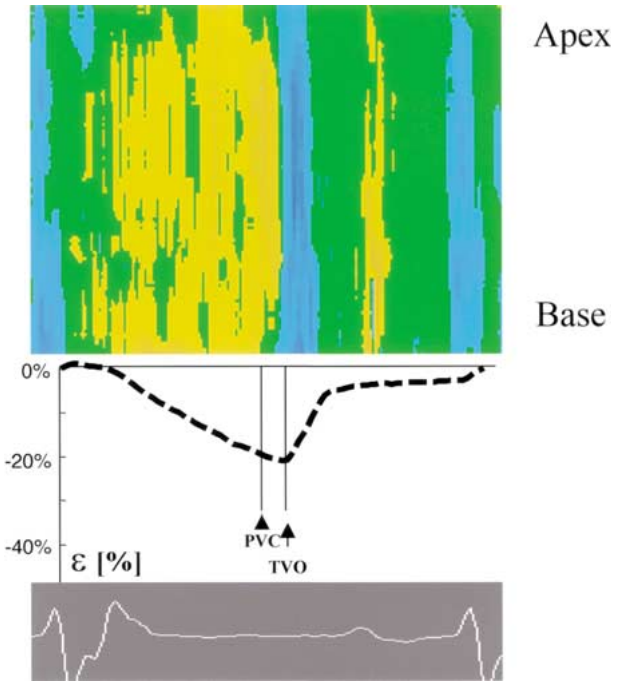

Fig. 10. An example of SR and ε data from a 12-year-old child 11 years post correction of a Fallot tetralogy with persistent moderate pulmonary insufficiency. **Top:** A long axis color-curved SR M-mode of the RV free wall from the apex to the base. The patchy yellow pattern in systole represents decreased myocardial shortening and the blue bands represents myocardial lengthening in early and late diastole with a long period of diastasis with almost no deformation (green band). **Bottom:** The ε curve extracted from the mid RV free wall. Note the very low systolic ε of only -20% (normal systolic $\varepsilon = -45 \pm 15\%$). *PVC*, pulmonary valve closure; *RV*, right ventricular; *TVO*, tricuspid valve opening; ε = strain.

Thus for the very apical region, longitudinal measurements are sometimes not possible. For the radial direction, only SR/ε in posterior wall segments can be measured.

A bigger problem lies in avoiding noise in the data set. *SR* is derived from comparison of two myocardial Doppler velocity data sets, and the calculation involved amplifies any noise component in other data sets. However this normally does not present a major problem in pediatric patients. Data averaging techniques and high frame rate data acquisition (>150/s) both help reduce the random noise component in SR/ε imaging.

Future Perspectives for DMI and Strain Rate/Strain Imaging

From the above, it would appear that both DMI velocity and SR/ε imaging could have important clinical applications in quantifying regional LV and RV function in pediatric cardiology. As *SR* imaging is less influenced by overall cardiac motion tethering effects than regional velocities, it should be superior to DMI velocity data in quantifying regional deformation. In the future, this methodology may be used to monitor myocardial function pre- and postcardiac intervention and during cardiotoxic drug therapy. *SR* imaging may also be useful in patients after cardiac transplantation by providing a new modality for quantifying wall deformation and assisting in the noninvasive evaluation of transplant rejection. In addition, this methodology may be used as a non invasive approach to quantify the deformation properties of hypertrophic and dilated cardiomyopathies in children and thus to better understand the pathophysiology of these diseases.

Further major technical developments to improve the methodology are possible. In the future it is likely that *SR* and ε will be calculated by cross-correlation methods based on radio frequency data [5]. This will have the advantage of markedly increasing the spatial resolution of the data in both the axial and lateral directions and will also allow the possibility of real time two-dimensional ε estimation [5].

Despite these encouraging results, further clinical studies are necessary to determine the precise clinical role of ultrasound based SR/ε imaging in quantifying regional function in pediatric cardiology.

The Interrelation of Regional Integrated Backscatter and Regional Myocardial One- and Two-Dimensional Strains

Integrated backscatter is a measure of the reflected ultrasound energy from a defined region of myocardium. Absolute integrated backscatter levels cannot be measured in clinical practice, but relative changes in levels during the cardiac cycle can. The normal variation in relative backscatter levels during myocardial contraction and relaxation has been termed the cyclic variation in integrated backscatter (CVIB). The normal changes in CVIB have been determined for radial deformation of septal and posterior wall segments. These have been described in both experimental and clinical studies. Normally, levels of radial CVIB are maximal in late diastole and minimal in late systole [1]. In addition, there is a transmural inhetero genicity in radial CVIB levels in normal myo cardium with maximal levels being recorded subendocardially and minimal levels subepicardially [3]. It should be noted at this point that little is known about regional long axis CVIB levels in either health

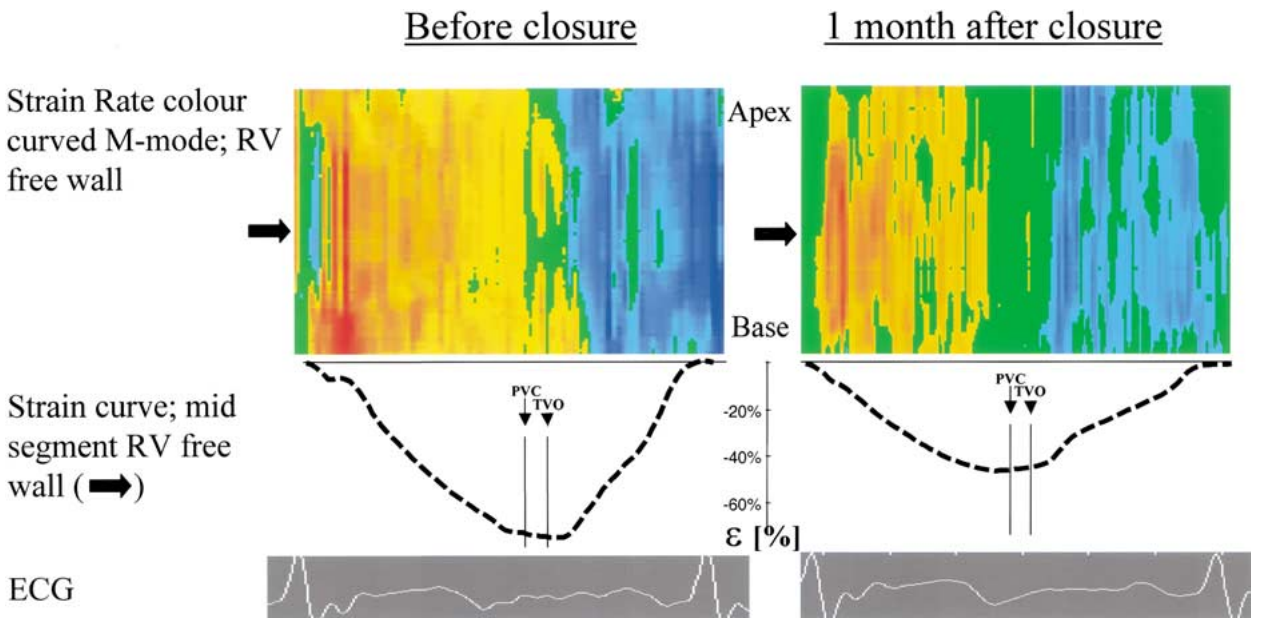

Fig. 11. An example of changes in *SR* and ε pre– and post–Amplatz device closure from 4-year-old child with a large atrial septal defect and large left to right shunt. **Left upper panel:** The long axis curved *SR* M-mode from the RV free wall. The dark orange band represents the increased myocardial shortening in systole, and the dark blue band represents the increased myocardial lengthening in early and late diastole. **Left lower panel:** The ε curve extracted from the mid RV free wall. Note the high systolic ε of −74% (normal systolic ε = −45 ± 15%). **Right:** One month after closure of the atrial septal defect. The corresponding long axis colol-curved *SR* M-mode of the RV free wall and ε curve from the mid RV free wall. Note that systolic e is now normal (−45%). PVC = pulmonary valve closure; RV = right ventricular; TVO = tricuspid valve opening; ε = strain.

or disease. However, the little data available would appear to show that there is a phase shift in long axis CVIB levels compared to radial data, with maximal long axis levels occurring at end systole and minimal levels during late diastole [2].

There has been much discussion on the precise mechanics underlying this CVIB. Rijsterborgh et al. in their experimental studies into radial CVIB suggested that the most important factor determining local changes in CVIB was radial deformation. This correlated best with changes in unidimensional deformation as measured either by microcrystals or by M-mode echocardiography [23, 24]. In a recent clinical study, Bijnens et al. [1] have compared normal changes in radial CVIB with radial two-dimensional strain calculated from an ultrasound RF data set and found an excellent correlation between the two (Fig. 13). They conclude that a major determinant of CVIB would appear to be changes in local two-dimensional ε. This would explain both the transmural inheterogenicity of radial CVIB values across the septum and the posterior wall in normal myocardium and could explain the amplitude and timing changes in normal peak integrated backscatter levels induced by acute ischemia. If this hypothesis is correct—and as the signal processing involved in deriving regional ε values is currently much simpler than measuring CVIB and ultrasound-derived

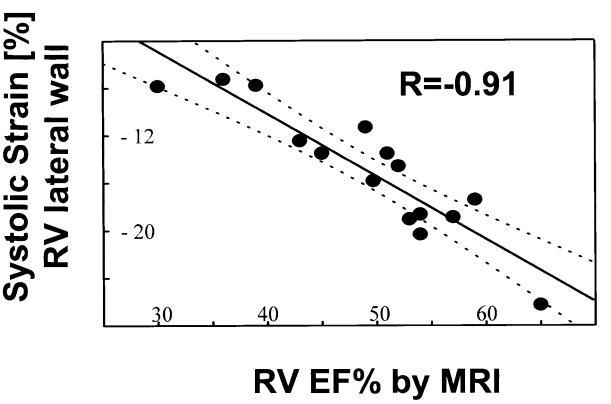

Fig. 12. The correlation of regional long axis systolic ε values derived from the basal RV free wall with the global RV ejection fraction assessed by MRI in a study in 15 post-Senning patients with homogenous SR curves in the RV free wall despite a wide variation in RV function. EF, ejection fraction; RV, right ventricular.

long axis ε values are relatively easy to obtain for long axis deformation for all LV and RV segments—it may be simpler and more robust to measure regional one or two-dimensional ε. However, further experimental and clinical studies are required to verify the correlation between local CVIB and ε over a range of myocardial pathologies.

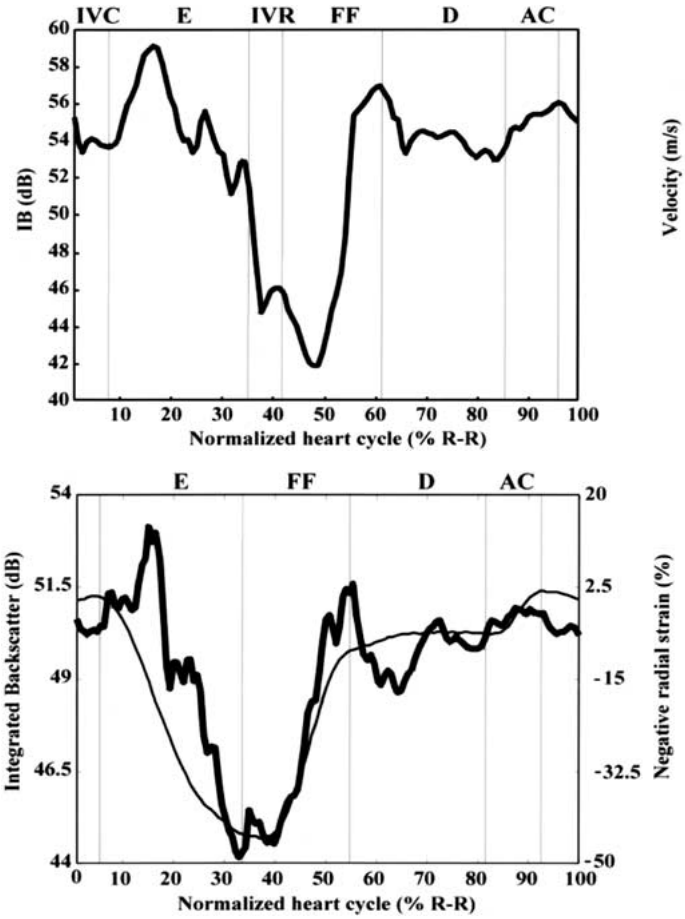

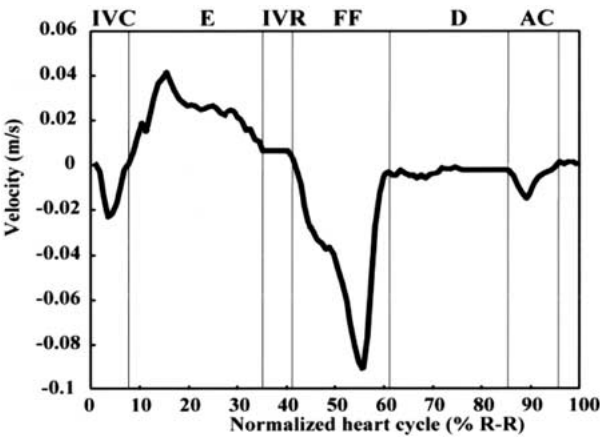

Fig. 13. An example of regional radial CVIB versus radial ε. **Upper left:** A regional radial DMI velocity curve derived from the basal posterior wall of a normal subject. **Upper right:** The radial CVIB curve averaged across the whole width of the basal posterior LV wall. **Bottom:** Thick line, the normal CVIB from a posterior wall segment. Thin line, the regional ε curve derived from the same ultrasound data set. Note how the CVIB curve parallels the ε curve. *AC*, atrial contraction; *D*, diastasis; *E*, ejection; *FF*, fast filling; *IB*, integrated backscatter; *IVC*, isovolumetric contraction; *IVR*, isovolumetric relaxation.

Acknowledgments. We thank Professor M. Gewillig and Dr. L. Mertens from the Department of Pediatric Cardiology, University Hospital Gasthuisberg, for their help in preparing this manuscript.

References

1. Bijnens B, D'Hooge J, Sutherland G, et al. (1999) Robustness of integrated backscatter for myocardial tissue characterization. *Ultrasound Med Biol 25*:95–103
2. Bouki KP, Lange A, Palka P, et al. (1996) Regional variations of ultrasonic integrated backscatter in normal and myopathic left ventricles. A new multi-view approach. *Eur Heart J 17*: 1747–1775
3. Colonna P, Montisci R, Galiuto L, Meloni L, Iliceto S (1999) Effects of acute myocardial ischemia on intramyocardial contraction heterogeneity: a study performed with ultrasound integrated backscatter during transesophageal atrial pacing. *Circulation 100*:1770–1776
4. D'Hooge J, Heimdal A, Jamal F, et al., (2000) Regional strain and strain rate measurements by cardiac ultrasound: principles, implementation and limitations. *Eur J Echocardiography 1*:154–l70
5. D'Hooge J, Konofagou E, Bijnens B, et al. (2000) Cardiac elastography—a feasibility study. (Abstr.) *Eur J Echocardiography Euroecho 4*:72 (Abstr)
6. Edvardson T, Skulstad H, Aakhus S, Urheim S, Ihlen H (2001) Regional myocardial systolic function during acute myocardial ischemia assessed by strain Doppler echocardiography. *J Am Coll Cardiol 37*:726–730
7. Fleming AD, Xia X, McDicken WN, Sutherland GR, Fenn L (1994) Myocardial velocity gradients detected by Doppler imaging. *Br J Radiol 67*:679–688
8. Gorcsan J III, Strum DP, Mandarino WA, Gulati VK, Pinsky MR (1997) Quantitative assessment of alterations in regional left ventricular contractility with color-coded tissue Doppler echocardiography. Comparison with sonomicrometry and pressure-volume relations. *Circulation 95*(10):2423–2433
9. Gutgesell HP (1985) Echocardiographic assessment of cardiac function in infants and children. *J Am Coll Cardiol 5*(1 Suppl):95S–103S
10. Hayabuchi Y, Matsuoka S, Kubo M, Kuroda Y (1998) Usefulness of color kinesis imaging for evaluation of regional right ventricular wall motion in patients with surgically repaired tetralogy of Fallot. *Am J Cardiol 82*:1224–1229
11. Heimdal A, Stoylen A, Torp H, Skjaerpe T (1998) Real-time strain rate imaging of the left ventricle by ultrasound. *J Am Soc Echocardiogr 11*: 1013–1019
12. Heimdal A, D'Hooge J, Bijnens B, Sutherland GR, Torp H (1998) In vitro validation of in-plane strain rate imaging. A new ultrasound technique for evaluating regional myocardial deformation based on tissue Doppler imaging. (Abstr.) *Echocardiography 15*(8):s40

13. Iwasaki Y, Satomi G, Yasukochi S (1999) Analysis of ventricular septal motion by Doppler tissue imaging in atrial septal defect and normal heart. *Am J Cardiol 83*(2):206–210
14. Jamal F, Kukulski T, D'Hooge J, De Scheerder I, Sutherland G (1999) Abnormal postsystolic thickening in acutely ischemic myocardium during coronary angioplasty: a velocity, strain, and strain rate Doppler myocardial imaging study. *J Am Soc Echocardiogr 12*:994–996
15. Jamal F, Kukulski T, Strotmann J, et al. (2001) Quantitation of the spectrum of changes in regional myocardial function during acute ischaemia in closed-chest pigs. An ultrasonic strain rate and strain study. *J Am Soc Echocardiogr* in press
16. Kapusta L, Thijssen JM, Cuypers MH, Peer PG, Daniels O (2000) Assessment of myocardial velocities in healthy children using tissue Doppler imaging. *Ultrasound Med Biol 26*:229–237
17. Kapusta L, Thijssen JM, Groot-Loonen J, et al. (2000) Tissue Doppler imaging in detection of myocardial dysfunction in survivors of childhood cancer treated with anthracyclines. *Ultrasound Med Biol 26*:1099–1108
18. Mertens L, Weidemann F, Sutherland GR (2001) Left ventricular function in abnormal left coronary artery arising from the pulmonary artery pre and post repair: The potential benefits of Ultrasound-based regional strain and strain rate imaging. *Cardiol Young 11*:79–83
19. Miyatake K, Yamagishi M, Tanaka N, et al. (1995) New method for evaluating left ventricular wall motion by color-coded tissue Doppler imaging: in vitro and in vivo studies. *J Am Coll Cardiol 25*:717–724
20. Mori K, Hayabuchi Y, Kuroda Y, Nii M, Manabe T (2000) Left ventricular wall motion velocities in healthy children measured by pulsed wave doppler tissue echocardiography: normal values and relation to age and heart rate. *J Am Soc Echocardiogr 13*(11): 1002–1011
21. Pacileo G, De Cristofaro M, Russo MG, et al. (2000) Hypertrophic cardiomyopathy in pediatric patients: effect of verapamil on regional and global left ventricular diastolic function. *Can J Cardiol 16*(2):146–152
22. Picano E, Lattanzi F, Orlandini A, Marini C, L'Abbate A. (1991) Stress echocardiography and the human factor: the importance of being expert. *J Am Coll Cardiol 17*:666–669
23. Rijsterborgh H, Mastik F, Lancee CT, et al. (1990) Ultrasonic myocardial integrated backscatter and myocardial wall thickness in animal experiments. *Ultrasound Med Biol 16*:29–36
24. Rijsterborgh H, Mastik F, Lancee CT, et al. The relative contributions of myocardial wall thickness and ischemia to ultrasonic myocardial integrated backscatter during experimental ischemia. *Ultrasound Med Biol 17*:41–48
25. Rychik J, Tian ZY (1996) Quantitative assessment of myocardial tissue velocities in normal children with Doppler tissue imaging. *Am J Cardiol 77*:1254–1257.
26. Sutherland GR, Stewart MJ, Groundstroem KW, et al. (1994) Color Doppler myocardial imaging: a new technique for the assessment of myocardial function. *J Am Soc Echocardiogr 7*(5):441–458
27. Urheim S, Edvardsen T, Torp T, Angelsen B, Smiseth O (2001) Myocardial strain by Doppler echocardiography. Validation of a new method to quantify regional myocardial function. *Circulation 102*:1158–1164
28. Vogel M, Yates R, Deanfield J, Redington AN (2000) Incoordinate wall motion detected by tissue Doppler imaging in patients after the Fontan operation. (Abstr.) *Cardiol Young 10*:42
29. Vogel M, Sponring J, Cullen S, Deanfield JE, Redington AN (2001) Regional wall motion and abnormalities of electrical depolarization and repolarization in patients after surgical repair of tetralogy of fallot. *Circulation 103*:1669–1673
30. Voigt JU, Arnold M, Karlsson M, et al. (2000) Assessment of regional long axis strain rate derived from Doppler myocardial imaging indices in normal and infarcted myocardium. *J Am Soc Echocardiogr* 13(6):588–598
31. Weidemann F, Eyskens B, Jamal F, et al. (2000) Regional strain distribution in the right ventricle after Senning repair for d-transposition of the great arteries. A color Doppler myocardial imaging study. (Abstr.) *Eur Heart J 21*(Suppl):616
32. Weidemann F, Jamal F, Mertens L, et al. (2000) Regional strain distribution throughout the left and right ventricle in healthy children. A color Doppler myocardial imaging study. A new cardiac ultrasound index of Regional deformation. (Abstr.) *Circulation*